Raman spectroscopy investigation of the H content of heated hard amorphous carbon layers

C. Pardanaud[a], C. Martin[a], P. Roubin[a], G. Giacometti[a],
C. Hopf[b], T. Schwarz-Selinger[b], W. Jacob[b].
[a] *Aix-Marseille Université, CNRS, PIIM UMR 7345, 13397 Marseille cedex 20, France.*
[b] *MPI für Plasmaphysik, EURATOM Association, Boltzmannstr. 2, 85748 Garching, Germany.*

Abstract

We revisit here how Raman spectroscopy can be used to estimate the H content in hard hydrogenated amorphous carbon layers. The H content was varied from 2 at.% to 30 at.%, using heat treatments of a a-C:H, from room temperature to 1300 K and was determined independently using ion beam analysis. We examine the correlation of various Raman parameters and the consistency of their thermal evolution with thermo-desorption results. We identify a weak band at 860 cm^{-1} attributed to H bonded to $C(sp^2)$. We show that the H_D/H_G parameter (Height ratio between the D and G bands) is quasi-linear in the full range of H content and can thus be used to estimate the H content. Conversely, we show that the m/H_G parameter (ratio between the photoluminescence background, m, and the height of the G band), often used to estimate the H content, should be used with care, first because it is sensitive to various photoluminescence quenching processes and second because it is not sensitive to H bonded to $C(sp^2)$.

Keywords: Amorphous hydrogenated carbon, Raman spectroscopy, Hydrogen retention

Published in:	Diamond and Related Materials, **34**, 100–104 (2013)
doi:	10.1016/j.diamond.2013.02.009
Submitted:	21.09.2012
Accepted:	19.02.2013
Available online	26.02.2013

1. Introduction

Raman spectroscopy is routinely used to characterize C-based materials. Interpreting the 1000 - 1800 cm^{-1} spectral region gives information on the carbon hybridization. The G band is due to the bond stretching of both aromatic and aliphatic $C(sp^2)$-$C(sp^2)$ pairs, whereas the D band (sometimes accompanied by a D' band) is due to the breathing of aromatic rings and is activated by the presence of defects [1]. They contain information on disorder such as the size of aromatic domains, the existence of $C(sp^3)$ in the neighborhood of $C(sp^2)$ and the H content [1-5]. The Raman parameters generally used to probe the structure are: the peak wavenumber and the width of the G and D bands, denoted $\square_{G,D}$ and $\square_{G,D}$ respectively, and the peak height ratio of these two bands, H_D/H_G [2]. Note that we note this ratio H_D/H_G to avoid confusion with I_D/I_G which would correspond to the integrated height ratio (intensity ratio). Depending on the kind of material, these parameters were found to be correlated [6, 7]. The D band peak height was found to be correlated with the H content in graphane [8].

For a-C:H layers, an additional spectral feature has to be taken into account: a photoluminescence background which is superimposed on the Raman spectrum. The slope of this background, m, is calculated between 800 and 2000 cm^{-1}. The higher m, the higher is the photoluminescence intensity. Electron-hole pairs are created by the laser used to produce the Raman effect. Relaxation in a-C:H then occurs following two competitive ways: photoluminescence and non-radiative recombination. The former process arises from the radiative recombination of the electron-hole pairs trapped in band tail states whereas the latter process can be due to the existence of paramagnetic dangling bonds inside the material. As the result of the competition between these two mechanisms, photoluminescence can be more or less quenched. Passivating these bonds, for example with hydrogen, removes this quenching [9]. Passivation can be done by annealing at low temperature ($T < 600$ K) which allows structural reorganization to occur [10, 11]. There is an alternative explanation of photoluminescence [12]: embedding 6-fold $C(sp^2)$ rings with different molecular conformation in a $C(sp^3)$ bonded network leads to create defect energy levels in the $\square$ and $\square^*$ electronic bands. Among several conformations, the distorted boat configuration of the 6-fold $C(sp^2)$ ring has an energy of 2.3 eV and can give rise to photoluminescence. In the two cases, defects due to the presence of $C(sp^3)$ (or $C(sp^3)$-like) are driving photoluminescence processes. This assumption is supported by the results found in [5] were the authors have correlated the $C(sp^3)/C(sp^2)$ to the slope of the photoluminescence background.

The m/H_G parameter measured with a 2.54 eV ($\square_L$ = 514.5 nm) laser is nevertheless often used to estimate the H content by comparison with an empirical linear law determined in [6] where the authors used numerous kinds of a-C:H layers. It was found that this parameter is linked to the hydrogen content of a-C:H layers by a linear relation: $H/H+C = 21.7 + 16.6 \log_{10} (m/H_G)$. Recently a similar linear relation has been found although with different coefficients [13]. The lowest H contents measured with this technique are H/H+C ~ 20 at.%.

We revisit here the H content determination of a heated hard a-C:H layers by means of Raman spectroscopy. Then, we analyze the evolution of Raman parameters with the structural and chemical changes under heat treatment from room temperature to 1300 K, the H content thus varying from 30 at.% to 2 at.%. Ion Beam Analyses (IBA) were used to determine the H content and Thermo-Desorption Spectrometry (TDS) was used to characterize the H release.

2. Experimental

A 220 nm thick hard amorphous, hydrogenated carbon thin films (a-C:H) was deposited on a Si wafer (10 cm in diameter) on the driven electrode of a capacitively coupled radio frequency plasma (13.56 MHz) in pure methane at 2 Pa and a DC self bias of -300V. Under very similar conditions, typical hard a-C:H layers with H/H+C ~ 30 at.% and mass density ~ 1.9 g cm^{-3} are formed [14]. To vary the hydrogen content, the wafer was cut in several samples about 1 cm^2.

Different samples were heat treated under ultra high vacuum conditions at selected annealing temperatures for ~ 60 minutes each. The annealing temperatures were varied from 400 to 1300 K. The as deposited layer will be called hereafter AD layer and the heat treated samples will be called hereafter HT samples. A helium bombarded Highly Oriented Pyrolytic Graphite (HOPG) was also used as reference (~ 800 eV, ~ 10^{18} cm^{-2}, see [15] for details).

Raman spectra were obtained at room temperature with a Horiba-Jobin-Yvon HR LabRAM apparatus (laser wavelength λ_L = 514.5 nm, 100X objective, resolution ~1 cm^{-1}, probe spot ~ 1 μm^2). The laser power was chosen as P ~ 0.2 mW m^{-2} to prevent damaging of the samples. A 100 second integration time was sufficient to obtain a good signal to noise ratio in the 1000 - 1800 cm^{-1} range whereas 1250 seconds were needed in the 350 - 900 cm^{-1} range. The main Raman parameters analyzed were the G peak wavenumber, ν_G, its full-width at half-maximum, Γ_G, the relative heights of the G and D bands, H_D/H_G, and the m/H_G ratio. A linear background was subtracted (slope m) and heights H_D and H_G were measured without any fitting to prevent from ambiguousness due to a model-dependent fitting procedure. H_D was therefore measured at its apparent maximum, except for the AD layer and the 600 K HT sample, for which the D band maximum was not well enough defined (see Fig. 1). For these two samples H_D was taken at 1370 cm^{-1}. Note that Γ_G will not be discussed in what follows as it follows the same behavior as ν_G [16].

The H/(H+C) ratio of the layers was determined by IBA. The use of a 3 MeV ^3He ion beam under an impact angle of 75° with respect to the surface normal allowed for the simultaneous measurement of ^1H in the sample via elastic recoil detection and of ^{12}C via nuclear reaction analysis using the $^{12}C(^3He,p)^{14}N$ reaction. Only the relative changes of the H and C areal densities were determined with respect to the as-deposited sample for which H/(H+C) = 0.3 was assumed. This value has been obtained previously on non-heat-treated samples deposited under conditions almost identical to those used in this work using an absolute quantification procedure that invoked calibration samples. Error bars of H/(H+C) for HT samples were estimated less than 2%.

Hydrogen release during heating was quantified by TDS. An as-deposited sample was heated from room temperature to 1350 K in a quartz tube immersed in a tube furnace at a heating rate of 15 K/min and the signals of various desorbing species, especially the signals at m/q = 2 and 16 that mostly originate from H_2 and CH_4, were recorded by a remote quadrupole mass spectrometer, [17].

3. Results and discussion

3.1 Thermal evolution of Raman spectra

Fig. 1.a displays the Raman spectra of the AD layer and the HT samples in the spectral range 1000 - 1800 cm^{-1}. The Raman spectrum of the AD layer is composed of a G band, situated at 1522 cm^{-1}, and a broad shoulder at ~ 1200 – 1400 cm^{-1} containing the D band. Upon heating up to 825 K, the G band narrows and blue shifts by 78 cm^{-1}. For higher annealing temperatures the G band position remains constant. Such a blue shift has been attributed to an aromatization occurring when annealing from room temperature and 1025 K by correlating X-ray photoemission spectroscopy with Raman spectroscopy [18]. On the other hand, for as deposited hard layers of various $C(sp^3)/C(sp^2)$ ratio, it has been shown by correlating electron energy loss spectroscopy with Raman spectroscopy that the larger the ν_G blue shift, the lower the $C(sp^3)$ content (figure 14 of [2]). Raman spectroscopy is sensitive mainly to $C(sp^2)$ bonds and therefore the $C(sp^3)$ which causes the shift is most probably situated in the neighborhood of a $C(sp^2)$ [3]. The D band intensity increases up to a value close to that of the G band at 1300 K. According to the amorphisation trajectory presented in [7], these evolutions reveal the organization of the material under heating, leading to larger aromatic clusters.

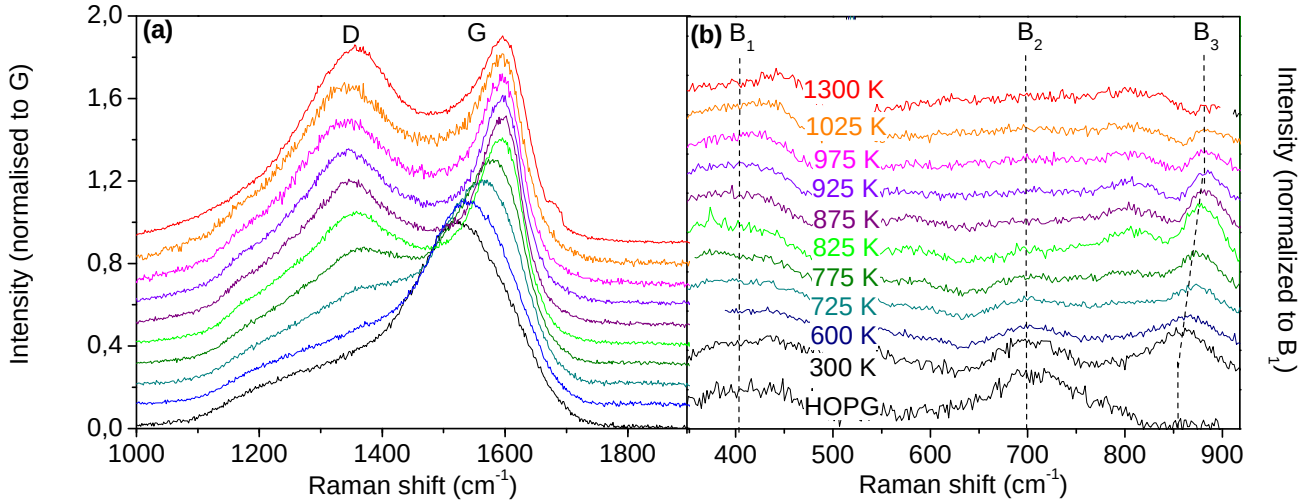

Figure 1: *Raman spectra of a plasma-deposited hard amorphous carbon layer, heat treated from room temperature to 1300 K (a) spectral range 1000 - 1800 cm^{-1} (a linear background was subtracted and spectra normalised) (b) spectral range 350-900 cm^{-1} (a linear background was subtracted). The spectrum at the bottom corresponds to He-bombarded HOPG (see text for details).*

Fig. 1b displays Raman spectra of the same samples in the 350-900 cm^{-1} spectral range for which a linear background was subtracted, comparing them with that of He bombarded HOPG. For graphene or graphite, this spectral range is usually silent because of Raman selection rules. Here, three weak and broad bands situated at 400, 700 and 860 cm^{-1} (called B_1, B_2 and B_3) are identified for the AD layer. Their intensity is very weak: less than ~ 4 % of that of the G band. B_1 and B_2 are present both for AD and He bombarded HOPG while B_3 is present only for AD. This suggests that B_3 is related to C-H bonds. Consistently, its frequency fits with those of polyaromatic hydrocarbon molecules C(sp^2)-H modes [19]. B_1 and B_2 frequencies are in the range of the phonon density of states of graphite (350 – 900 cm^{-1} [16]), and, although hard layers are far from pure graphite, these bands may correspond to phonons. B_1 and B_2 evolution with heating also differs from that of B_3 with respect to intensity, position and shape. When heating from room temperature to 1300 K, the intensity of B_1 remains roughly constant, varying from 2 % to 4 % of that of G independent of the temperature. Its profile remains broad and not well defined. The intensity of B_2 decreases from room temperature to 775 K and then B_2 stays like a plateau. Conversely, the profile of B_3 remains well defined upon heating. Its position clearly blue shifts by ~ 25 cm^{-1} up to 875 K and then remains constant while its intensity decreases continuously and vanishes at 1300 K.

Fig. 2a to 2c display the thermal evolution of $\square_G$ and $\square_{B3}$, m/H_G and H_D/H_G, respectively. They are compared to the H content as determined using IBA shown in Fig. 2c. Fig. 2a displays the evolution of $\square_G$ and $\square_{B3}$ as extracted from the spectra shown in Fig. 1a and 1b. The plateau of $\square_G$ above ~ 850 K means that the number of C(sp^3) neighboring C(sp^2) no longer changes. The thermal evolutions of the two bands are remarkably similar: this suggests that the C(sp^2)-H bond is sensitive to the presence of C(sp^3).

Fig. 2b shows that m/H_G increases by ~ 40% between 300 and 600 K and then decreases monotonically from 600 to 875 K where m/H_G ~ 0.05. For higher temperatures the slope m is approximately zero. On the other hand, Fig. 2c shows that between 300 and 600 K the H content is constant (H/H+C ~ 30 at.%). The increase of m/H_G is thus probably due to an increase of

photoluminescence (increasing m) due to aromatization and/or defect passivation occurring at the first stages of heating. Therefore, m/H_G cannot be simply related to the H content in this temperature range. At higher temperature, H/H+C decreases from 30 at.% down to ~2 at.%, without reaching a plateau.

Fig. 2c shows that H_D/H_G and H/H+C evolve in a remarkably symmetrical way, with H_D/H_G increasing continuously from ~ 0.4 to ~ 1 with T increasing from 300 to 1300 K. This suggests that the two parameters are correlated and that H_D/H_G could be used to probe the hydrogen content.

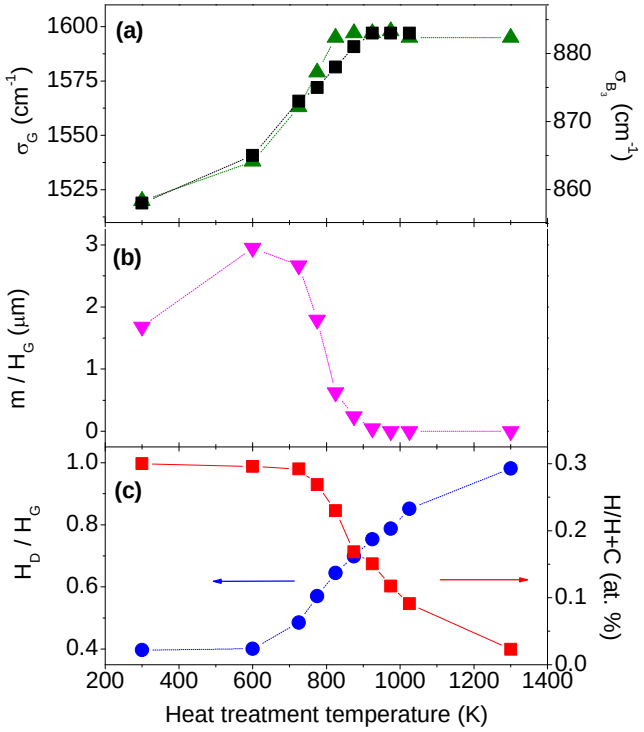

Figure 2: *Evolution of Raman parameters versus the heat treatment temperature: (a) σ_G (up triangle) and σ_{B3} (square) (b) m/H_G (down triangle) and (c) H_D/H_G (circle) compared to the H content determined by IBA (square).*

To summarize, the H content and the B_3 intensity continuously decrease up to 1300 K, while $\square_G$ and m/H_G remains constant for T > 850 K. As B_3 is attributed to C(sp^2)-H while the $\square_G$ shift and the photoluminescence are due to the presence of C(sp^3), the high temperature process up to 1300 K is thus likely correlated to H release from C(sp^2), while the low temperature process (300 – 850 K) is likely correlated to both aromatization and H release from C(sp^3). This is in agreement with the sequential destruction of C(sp^3)-H and C(sp^2)-H groups evidenced in samples with similar H content in [20], although the destruction temperatures of C(sp^3)-H and C(sp^2)-H groups are higher than in our study, up to 1040 and 1400 K, respectively. The evolution of $\square_G$ starts below 600 K while a significant H content decrease starts only at 700 K: this indicates that the material organization occurs before the H release.

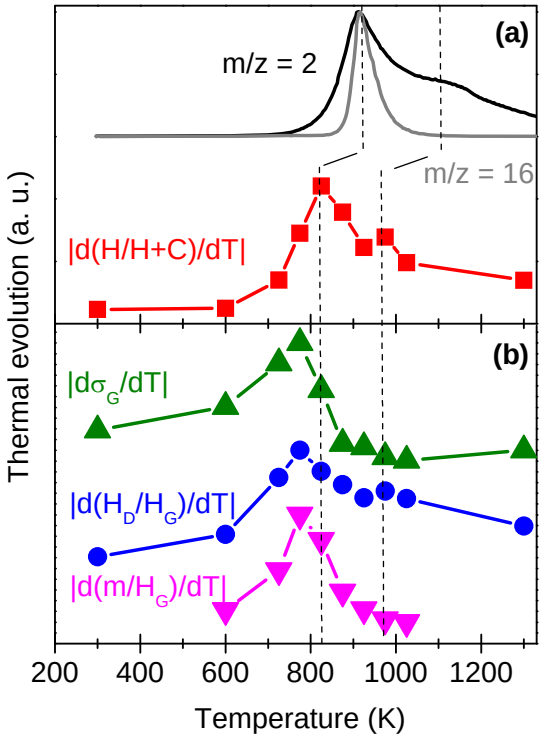

Figure 3: *AD and HT layers: (a) Thermodesorption spectrum of the AD layer and normalised absolute value of the derivative of the IBA thermal evolution of figure 2.c (b) normalised absolute values of the derivatives of the Raman parameter thermal evolutions of figure 2.a, 2.b and 2.c.*

3.2 Structure and H-content dependences of Raman parameters

Fig. 3.a displays the TDS measurements at mass 2 and mass 16 of the AD layer heated with a heating ramp of 15 K min^{-1}. Mass 2 and mass 16 correspond to H_2 and CH_4 which are known to be the dominant released species of this type of layer [17]. These measurements are compared to normalized absolute values of derivatives (versus the annealing temperature) of the H content measured by IBA (Fig. 3a) and of the Raman parameters, σ_G, H_D/H_G and m/H_G (Fig. 3b), as a function of the annealing temperature. The TDS signal of H_2 is composed of two contributions, centered at ~ 900 K and ~ 1100 K, whereas the TDS signal of CH_4 has only a contribution at ~ 900 K. These two contributions have been attributed to $C(sp^3)$-H and $C(sp^2)$-H, respectively [21]. Consistently, the temperature derivative of the H/H+C signal is also composed of two contributions, centered at ~ 825 K and ~ 975 K. The shift between these TDS and IBA results depends on the way the sample is heated, as suggested in [18]. In comparable TDS investigations it was shown that the peak maxima of the TDS peaks shift to lower temperatures if lower heating ramps are used (C. Hopf et al., to be published). H_D/H_G also displays these two contributions (at ~ 775 K and ~ 975 K) while σ_G and m/H_G do not. The comparison with the TDS spectrum thus strongly supports the analysis of Fig. 2 (section 3.1) and supports the supposition that H_D/H_G probes all the H content, i.e. both $C(sp^3)$-H and $C(sp^2)$-H, while m/H_G only probes $C(sp^3)$-H. Finally, note that the calculus of the derivative uses 50 K steps and therefore the observed shift (~ 50 K) of the Raman parameter maxima compared to that of the IBA signal has probably no physical meaning.

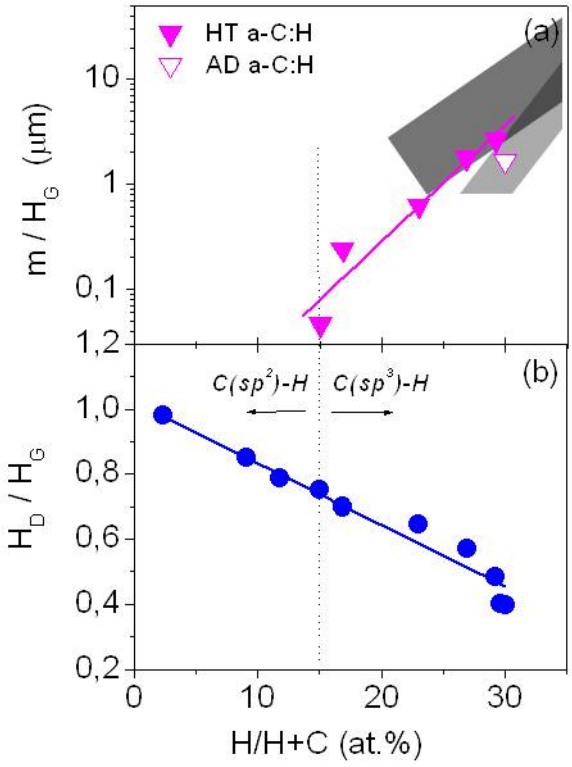

Figure 4: *H content estimation using Raman parameters: (a) m/H_G and (b) H_D/H_G as a function of H/H+C. Between 20 and 30 at.%, uncertainties of the band height are estimated to be around +/-0.025, error bars due to noise is ~0.005 in the overall H-content. Dark and light grey zones correspond to previously published data (respectively [6] and [13]).*

To summarize the presented results, Fig. 4a and 4b display m/H_G and H_D/H_G as a function of H/H+C. In logarithmic scale, m/H_G is well fitted by a linear relation: $H/H+C = A + B \log_{10}(m/H_G)$, with A = 25 and B = 9. Such a linear relation (although with different slopes) was previously obtained from a large set of samples [6, 13] leading to a significant spreading of data which are indicated in figure 4a by the grey zones. IBA probes all H in the film, i.e., both $C(sp^2)$-H and $C(sp^3)$-H, while m/H_G only probes $C(sp^3)$-H and this could explain the spreading of the data and the observation of different slopes, depending on the $C(sp^3)$-H / $C(sp^2)$-H ratio of the a-C:H layers investigated in Refs 6 and 13. Note that the AD layer point is off the straight line: this is related to the specific behavior of the m/H_G parameter at low temperature, which is sensitive not only to the H content but also to the behavior of defects possibly quenching the photoluminescence. For AD layers, various amounts of defects thus induce various m values that may explain the spreading observed for the data presented in Ref. 6. On the other hand, H_D/H_G is remarkably well fitted by a linear relation ($H/H+C = 0.54 - 0.53\ H_D/H_G$) from 2 at.% to 20 at.%. Between 20 and 30 at.%, the D band is not well-defined and strongly overlaps with the G band and the linear relation is thus less clear because of the uncertainties of the band height which are estimated to be around +/-0.025 (error bar due to noise is ~0.005). In addition, the material organization occurring together with the H release most probably also plays a role in the D band definition. Note that for samples with higher H-content (~ 40%), the D and G bands start to disappear contrary to the photoluminescence background. Depending of the H content, a combination of the two methods is thus needed for the H quantification.

It is well-known that for hard layers, electron properties are driven by the $C(sp^2)$ network whereas mechanical properties are driven by the $C(sp^3)$ network ([22] and references therein). The quasi-linear relation found here for H release from both $C(sp^2)$ and $C(sp^3)$ suggests that the $C(sp^2)$ and $C(sp^3)$ network and properties are intricated, aromatization being forced by $C(sp^3)$ or $C(sp^3)$-like defect.

4. Conclusion

Heat treatments of a hard type of a-C:H layer from room temperature up to 1300 K were performed and the hydrogen content evolution was studied by means of Raman spectroscopy, ion beam analyses and thermo-desorption spectroscopy. A good consistency between results from these three analyses has been found, allowing new information to be deduced from Raman spectra. We have analyzed the different heating stages with respect to structure and H content, and clarified how Raman parameters are correlated to the observed changes. In particular, the contributions of H bonded either to $C(sp^2)$ or to $C(sp^3)$ are emphasized and we show that Raman spectroscopy gives valuable information not only on structural properties but also on this type of chemical properties, leading to a consistent picture of what happens in the material: carbon organization starts below 600 K followed by H release from $C(sp^3)$ or $C(sp^3)$-like defect below 850 K and then by H release from $C(sp^2)$ at higher temperature. The relation of $\log_{10}(m/H_G)$ with the H content is found to be linear from 15 at.% to 30 at.%, extending the validity of this relation previously found for as deposited samples and for higher values of the H content. We emphasize here the limits of this relation first because the m/H_G signal (photoluminescence) is sensitive to defects and second because m/H_G is due to H bonded to $C(sp^3)$ or $C(sp^3)$-like defects. These two effects can lead to a misinterpretation of the H content. A linear relation is found between H_D/H_G and the total H content from 2 at.% to 20 at. %, due to H bonded to either $C(sp^2)$. For other hard a-C:H films with comparable initial structure, this statement may also be valid and this has to be confirmed. To better understand the different processes possibly involved such as H migration, H_2 and CH_4 formation, carbon organization, their kinetics at various temperatures are currently under study.

Acknowledgments

We acknowledge the Euratom-CEA association, the EFDA European Task Force on Plasma Wall Interactions, the Fédération de Recherche FR-FCM, the French agency ANR (ANR-06-BLAN-0008 contract) and the PACA Region (FORMICAT project) for financial support.

References

[1] F. Tuinstra, and J. L. Koenig, J. Chem. Phys. **53**, 1126 (1970).
[2] A. C. Ferrari, and J. Robertson, Phys. Rev. B **61**, 14095 (2000).
[3] J. Schwan *et al.*, J. Appl. Phys. **80**, 440 (1996).
[4] J. Choi *et al.*, Diam. Relat. Mat. **20**, 845 (2011).
[5] G. Adamopoulos *et al.*, J. Appl. Phys. **96**, 6348 (2004).
[6] C. Casiraghi, A. C. Ferrari, and J. Robertson, Phys. Rev. B **72**, 085401 (2005).
[7] A. C. Ferrari, and J. Robertson, Phys. Rev. B **64**, 075414 (2001).
[8] D. C. Elias *et al.*, Science **323**, 610 (2009).
[9] J. Robertson, Phys. Rev. B **53**, 16302 (1996).
[10] N. M. J. Conway *et al.*, Diamond relat. mater. **9**, 765 (2000).
[11] N. M. J. Conway *et al.*, Appl. Phys. Lett. **73**, 2456 (1998).
[12] M. Pandey, and D. S. Patil, Diam. Relat. Mat. **16**, 1912 (2007).
[13] J. G. Buijnsters *et al.*, J. Appl. Phys. **105**, 093510 (2009).
[14] T. Schwarz-Selinger, A. von Keudell, and W. Jacob, J. Appl. Phys. **86**, 3988 (1999).
[15] L. Schiesko *et al.*, Plasma Sources Science & Technology **17** (2008).
[16] C. Pardanaud *et al.*, J. Nucl. Mater. **415**, S254 (2011).
[17] E. Salançon *et al.*, J. Nucl. Mat. **376**, 160 (2008).
[18] S. Takabayashi *et al.*, J. Appl. Phys. **104**, 043512 (2008).
[19] A. Pathak, and S. Rastogi, Chem. Phys. **313**, 133 (2005).
[20] J. Biener *et al.*, Phys. Rev. B **49**, 17307 (1994).
[21] A. Schenk *et al.*, J. Appl. Phys. **77**, 2462 (1995).
[22] J. Robertson, Curr. Opin. Solid State Mat. Sci. **1**, 557 (1996).